2005-01-01

Network model for MIMO systems with coupled antennas and noisy amplifiers

Michael A. Jensen
jensen@byu.edu

Matthew L. Morris

Original Publication Citation

Morris, M. L., and M. A. Jensen. "Network Model for MIMO Systems with Coupled Antennas and Noisy Amplifiers." Antennas and Propagation, IEEE Transactions on 53.1 (25): 545-52

Network Model for MIMO Systems With Coupled Antennas and Noisy Amplifiers

Matthew L. Morris and Michael A. Jensen, *Senior Member, IEEE*

***Abstract*—This paper presents a framework for the analysis of mutually-coupled antennas in a multiple-input multiple-output system. The approach uses network theory to formulate the transfer matrix relating the signals input to the transmit antennas to the signals at the output of the receiver front end. This transfer function includes the coupled transmit and receive antennas, the multipath propagation channel, the receiver matching network, and a realistic noise model for the receive amplifiers. Application of the formulation to coupled dipole antennas characterized using full-wave electromagnetic analysis illustrates the performance gains possible from matching the coupled antenna/receive amplifier subsystem for minimum noise figure as compared to matching for maximum signal power transfer.**

***Index Terms*—Amplifier noise, multiple-input multiple-output (MIMO) systems, mutual coupling.**

I. Introduction

MULTIPLE-INPUT multiple-output (MIMO) communication systems use antenna arrays to increase communication capacity by exploiting the spatial properties of a multipath channel [1], [2]. Providing high capacity requires independence of the channel matrix coefficients, a condition generally achieved with wide antenna element spacings. For many subscriber units, such separations are unrealistic, and the resulting antenna mutual coupling [3] can impact communication performance.

Evaluating the impact of antenna mutual coupling on MIMO system performance has generally been approached by examining how the altered radiation patterns change the signal correlation [4], [5] and using this correlation to derive the system capacity [6]–[13]. However, this approach neglects the impact of transmit array coupling on the radiated power as well as the power collection capabilities of the coupled receive array connected through a matching network to the front-end amplifiers. Recent work has demonstrated how these additional considerations can be taken into account [14], [15]. However, in past studies the noise model for the receiver front end is overly simplistic. As a result, the prior observation that the optimal matching network should maximize power transfer is inappropriate for typical amplifier structures with more complex noise characteristics [14].

Manuscript received November 18, 2003; revised June 4, 2004. This work was supported by the National Science Foundation under Information Technology Research Grants CCR-0081476 and CCR-0313056.

The authors are with the Department of Electrical and Computer Engineering, Brigham Young University, Provo, UT 84602 USA (e-mail: jensen@ee.byu.edu).

Digital Object Identifier 10.1109/TAP.2004.838774

In this work, we use a detailed network model of a MIMO system to realistically account for mutual coupling and amplifier noise on the overall capacity. In conjunction with a path-based channel model, this formulation constructs the channel matrix relating the signals input to the transmit antennas to those at the output of the receiver front end and uses this result to compute the MIMO system capacity. Computational examples using coupled dipoles characterized using full-wave electromagnetic analysis reveal that matching the receiver amplifiers for minimum noise figure can lead to significant performance improvement over matching for optimal power transfer.

II. MIMO Network Model

Characterizing a complete MIMO communication system requires a model that includes the coupled transmit and receive antenna arrays, the multipath propagation channel, the receiver front-end matching network, and the terminated receiver amplifiers. Fig. 1 shows a block diagram of this system model. In this diagram and throughout the analysis, boldface uppercase and lowercase letters will describe matrices and column vectors, respectively, with H_{mn} denoting the element occupying the mth row and nth column of the matrix $\mathbf{H}$, and h_m representing the mth element of the vector $\mathbf{h}$. We use scattering parameters (S-parameters) referenced to a real impedance Z_0 [16] to describe the signal flow within the network wherein the forward and reverse traveling waves are denoted as $\mathbf{a}$ and $\mathbf{b}$, respectively. The flow diagram representation for the receiver network, with the network blocks delineated by dashed lines, appears in Fig. 2.

A. Coupled Arrays and Propagation Channel

We first consider a signal $\mathbf{a}_T$ that excites the transmit array consisting of N_T mutually-coupled antenna elements and characterized by an S-matrix $\mathbf{S}_{TT}$. The net power flowing into the network is $\|\mathbf{a}_T\|^2 - \|\mathbf{b}_T\|^2$ which, for lossless antennas, equals the instantaneous radiated transmit power P_T^{inst}. Since $\mathbf{b}_T = \mathbf{S}_{TT}\,\mathbf{a}_T$, we have

$$P_T^{\text{inst}} = \mathbf{a}_T^H \underbrace{\left(\mathbf{I} - \mathbf{S}_{TT}^H \mathbf{S}_{TT}\right)}_{\mathbf{A}} \mathbf{a}_T \tag{1}$$

where $\{\cdot\}^H$ is a conjugate transpose. For zero mean signals, the average radiated power is given by

$$P_T = E\left\{P_T^{\text{inst}}\right\} = \text{Tr}(\mathbf{R}_T\mathbf{A}) \tag{2}$$

where $\mathbf{R}_T = E\left\{\mathbf{a}_T\,\mathbf{a}_T^H\right\}$, $E\{\cdot\}$ denotes an expectation, and $\text{Tr}(\cdot)$ is the trace operation. The effect of this transmitted power

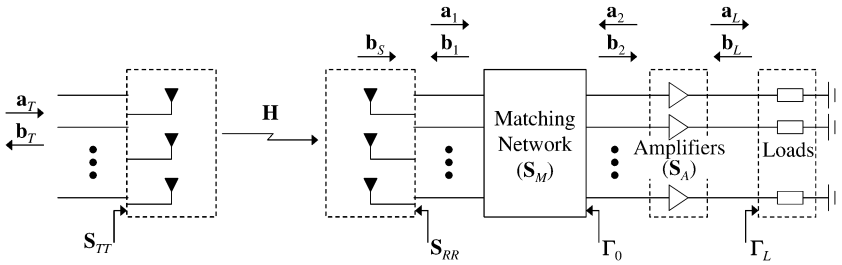

Fig. 1. Block diagram of the MIMO system including mutually coupled arrays, propagation channel, matching network, receiver amplifiers, and loads.

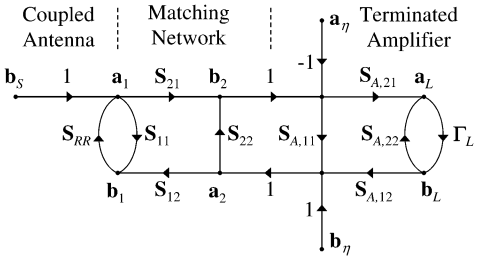

Fig. 2. Flow diagram representation of the MIMO receiver depicted in Fig. 1.

relation on the formulation of the capacity will be addressed in Section III.

The radiation pattern for the nth element of the transmit array for a unit driving current and all other elements in the array terminated in an open-circuit is denoted as $\mathbf{e}_{Tn}(\theta,\phi)$, where (θ,ϕ) represent the angular spherical coordinates referenced to the transmit array origin. The two elements of the column vector represent the $\hat{\theta}$ and $\hat{\phi}$ polarizations. The total transmitted field is then

$$\mathbf{e}_T(\theta,\phi)=\sum_{n=1}^{N_T}\mathbf{e}_{Tn}(\theta,\phi)i_{Tn}=\mathbf{E}_T(\theta,\phi)\mathbf{i}_T \tag{3}$$

where i_{Tn} is the excitation current on the nth antenna and $\mathbf{e}_{Tn}(\theta,\phi)$ is the nth column of the $2\times N_T$ matrix $\mathbf{E}_T(\theta,\phi)$.

We assume that the propagation channel between the transmit and receive arrays consists of a set of L plane waves, with the ℓth wave characterized by a complex voltage gain β_ℓ, angle of departure (AOD) $(\theta_{T\ell},\phi_{T\ell})$, and angle of arrival (AOA) $(\theta_{R\ell},\phi_{R\ell})$. We also assume that each plane wave undergoes a polarization transformation due to scattering that can be expressed as the unitary matrix

$$\mathbf{P}_\ell=\begin{bmatrix}p_{\ell,\theta\theta} & p_{\ell,\theta\phi}\\ p_{\ell,\phi\theta} & p_{\ell,\phi\phi}\end{bmatrix}. \tag{4}$$

Finally, we represent the radiation pattern of the mth coupled receive element $(1\le m\le N_R)$ referenced to the receiver coordinate origin as $\mathbf{e}_{Rm}(\theta,\phi)$. The open circuit voltage on the mth receive element is then given as

$$\begin{aligned}v_{Rm}&=\sum_{\ell=1}^{L}\mathbf{e}_{Rm}^T(\theta_{R\ell},\phi_{R\ell})\beta_\ell\mathbf{P}_\ell\sum_{n=1}^{N_T}\mathbf{e}_{Tn}(\theta_{T\ell},\phi_{T\ell})i_{Tn}\\&=\sum_{n=1}^{N_T}\underbrace{\sum_{\ell=1}^{L}\mathbf{e}_{Rm}^T(\theta_{R\ell},\phi_{R\ell})\beta_\ell\mathbf{P}_\ell\mathbf{e}_{Tn}(\theta_{T\ell},\phi_{T\ell})}_{2Z_0H_{mn}}i_{Tn}\end{aligned} \tag{5}$$

where $\{\cdot\}^T$ is a matrix transpose and the term $2Z_0$ is isolated for later convenience. The vector of received open-circuit voltages at the antenna terminals is then

$$\mathbf{v}_R=2Z_0\mathbf{H}\,\mathbf{i}_T. \tag{6}$$

B. Receive Antenna Port Output Signal

We are now poised to formulate an expression for the traveling wave delivered by the receive antenna terminals to a set of independent loads of resistance Z_0. Denoting this wave as $\mathbf{b}_S$, the antenna port signals for a general termination are related according to

$$\mathbf{a}_1=\mathbf{b}_S+\mathbf{S}_{RR}\mathbf{b}_1 \tag{7}$$

where we have used the notation of Figs. 1 and 2. For an open-circuit termination $(\mathbf{a}_1=\mathbf{b}_1)$, this yields

$$\mathbf{b}_S=(\mathbf{I}-\mathbf{S}_{RR})\mathbf{a}_1 \tag{8}$$

where $\mathbf{I}$ represents the identity matrix. Furthermore, the voltage at the open-circuit antenna terminals can be represented by $\mathbf{v}_R=Z_0^{1/2}(\mathbf{a}_1+\mathbf{b}_1)=2Z_0^{1/2}\mathbf{a}_1$. Equating this result to (6) and substitution into (8) leads to

$$\mathbf{b}_S=Z_0^{1/2}(\mathbf{I}-\mathbf{S}_{RR})\mathbf{H}\,\mathbf{i}_T. \tag{9}$$

Finally, since the transmit current can be expressed as $\mathbf{i}_T=Z_0^{-1/2}(\mathbf{a}_T-\mathbf{b}_T)=Z_0^{-1/2}(\mathbf{I}-\mathbf{S}_{TT})\mathbf{a}_T$, we obtain

$$\mathbf{b}_s=\underbrace{(\mathbf{I}-\mathbf{S}_{RR})\mathbf{H}(\mathbf{I}-\mathbf{S}_{TT})}_{\mathbf{S}_{RT}}\mathbf{a}_T. \tag{10}$$

C. Matching Network Output Signal

Given the multiport nature of the receiving system, the matching network will be represented using a block matrix S-parameter description, or

$$\mathbf{S}_M=\begin{bmatrix}\mathbf{S}_{11} & \mathbf{S}_{12}\\ \mathbf{S}_{21} & \mathbf{S}_{22}\end{bmatrix} \tag{11}$$

where 1 and 2 refer to input and output ports, respectively. With this notation, the signal $\mathbf{b}_2$ at the matching network output can be determined using network theory. To begin, we use (7) with $\mathbf{b}_1=\mathbf{S}_{11}\mathbf{a}_1+\mathbf{S}_{12}\mathbf{a}_2$ to obtain

$$\mathbf{a}_1=\left(\mathbf{I}-\mathbf{S}_{RR}\mathbf{S}_{11}\right)^{-1}\left(\mathbf{b}_S+\mathbf{S}_{RR}\mathbf{S}_{12}\mathbf{a}_2\right). \tag{12}$$

Since $\mathbf{b}_2 = \mathbf{S}_{21}\mathbf{a}_1 + \mathbf{S}_{22}\mathbf{a}_2$ we have

$$\mathbf{b}_2 = \mathbf{S}_{21}\left(\mathbf{I} - \mathbf{S}_{RR}\mathbf{S}_{11}\right)^{-1}\mathbf{b}_S + \underbrace{\left[\mathbf{S}_{22} + \mathbf{S}_{21}\left(\mathbf{I} - \mathbf{S}_{RR}\mathbf{S}_{11}\right)^{-1}\mathbf{S}_{RR}\mathbf{S}_{12}\right]}_{\boldsymbol{\Gamma}_0}\mathbf{a}_2 \quad (13)$$

where we have used $\boldsymbol{\Gamma}_0$ to represent the reflection coefficient at the matching network output (see Fig. 1).

D. Noisy Amplifier Output Signal

The added complication considered in this paper is the noise model associated with practical high-frequency transistor based amplifiers. To maintain tractability in the analysis, we will consider amplifier topologies that can be described by input-output S-parameters and standard noise parameters. This data can be readily obtained from manufacturer specifications on transistors designed for low-noise amplifier applications [17].

For the equivalent model adopted in this work, the mth noisy amplifier injects forward and reverse traveling noise waves $a_{\eta,m}$ and $b_{\eta,m}$, respectively, at the amplifier input [18]. Using the notation of Fig. 2, the amplifier signal-plus-noise output waves are of the form

$$\mathbf{a}_2 = \mathbf{S}_{A,11}\mathbf{b}_2 + \mathbf{S}_{A,12}\mathbf{b}_L - \mathbf{S}_{A,11}\mathbf{a}_\eta + \mathbf{b}_\eta \quad (14)$$

$$\mathbf{a}_L = \mathbf{S}_{A,21}\mathbf{b}_2 + \mathbf{S}_{A,22}\mathbf{b}_L - \mathbf{S}_{A,21}\mathbf{a}_\eta \quad (15)$$

where the subscript "A" denotes the S-parameters of the amplifiers. It is the introduction of the reverse traveling noise wave $\mathbf{b}_\eta$ that significantly alters this analysis relative to prior work and that generally leads to different conclusions regarding the impact of the matching network and the optimal achievable performance.

Inserting (14) with $\mathbf{b}_L = \boldsymbol{\Gamma}_L\mathbf{a}_L$ into (13) leads to

$$\mathbf{b}_2 = \left(\mathbf{I} - \boldsymbol{\Gamma}_0\mathbf{S}_{A,11}\right)^{-1}\Big[\mathbf{S}_{21}\left(\mathbf{I} - \mathbf{S}_{RR}\mathbf{S}_{11}\right)^{-1}\mathbf{b}_S + \boldsymbol{\Gamma}_0\left(\mathbf{b}_\eta - \mathbf{S}_{A,11}\mathbf{a}_\eta + \mathbf{S}_{A,12}\boldsymbol{\Gamma}_L\mathbf{a}_L\right)\Big]. \quad (16)$$

Since $\mathbf{a}_L = \mathbf{S}_{A,21}(\mathbf{b}_2 - \mathbf{a}_\eta) + \mathbf{S}_{A,22}\boldsymbol{\Gamma}_L\mathbf{a}_L$, we obtain

$$\mathbf{a}_L = \left(\mathbf{I} - \mathbf{S}_{A,22}\boldsymbol{\Gamma}_L\right)^{-1}\mathbf{S}_{A,21}\left(\mathbf{b}_2 - \mathbf{a}_\eta\right). \quad (17)$$

Substituting (16) into (17) and simplifying and subsequently using the fact that the voltage across the load is $\mathbf{v}_L = Z_0^{1/2}(\mathbf{I} + \boldsymbol{\Gamma}_L)\mathbf{a}_L$ leads to the expression

$$\mathbf{v}_L = \mathbf{Q}[\underbrace{\mathbf{S}_{21}\left(\mathbf{I} - \mathbf{S}_{RR}\mathbf{S}_{11}\right)^{-1}}_{\mathbf{G}}\mathbf{b}_S + \bar{\boldsymbol{\Gamma}}_0\mathbf{b}_\eta - \mathbf{a}_\eta] \quad (18)$$

where

$$\mathbf{Q} = Z_0^{1/2}\left(\mathbf{I} + \boldsymbol{\Gamma}_L\right)\Big[\left(\mathbf{I} - \boldsymbol{\Gamma}_0\mathbf{S}_{A,11}\right)\mathbf{S}_{A,21}^{-1}\left(\mathbf{I} - \mathbf{S}_{A,22}\boldsymbol{\Gamma}_L\right) - \boldsymbol{\Gamma}_0\mathbf{S}_{A,12}\boldsymbol{\Gamma}_L\Big]^{-1}. \quad (19)$$

Finally, using the expression in (10) leads to the final form of the load voltage

$$\mathbf{v}_L = \mathbf{Q}\left[\mathbf{G}\mathbf{S}_{RT}\mathbf{a}_T + \boldsymbol{\Gamma}_0\mathbf{b}_\eta - \mathbf{a}_\eta\right]. \quad (20)$$

E. Matching Network Specification

Practical amplifier design involves specifying an amplifier performance goal and synthesizing the source and load terminations that achieve this goal. Signal amplifiers are typically designed to provide minimum noise figure, optimal power gain, or some compromise between the two [17]. Our main concern in this analysis, therefore, is to define a desired value of $\boldsymbol{\Gamma}_0$, which is the source termination seen by the amplifier, and use this value to determine the sub-blocks $\mathbf{S}_{ij}$ of the matching network.

We will restrict our discussion to lossless matching networks that ideally have unity noise figures and are characterized by unitary S-matrices. We can take the singular value decomposition (SVD) of the sub-blocks $\mathbf{S}_{ij} = \mathbf{U}_{ij}\boldsymbol{\Lambda}_{ij}^{1/2}\mathbf{V}_{ij}^H$ in (11), where $\mathbf{U}_{ij}$ and $\mathbf{V}_{ij}$ are unitary matrices of singular vectors and $\boldsymbol{\Lambda}_{ij}^{1/2}$ is a diagonal matrix of real singular values. Then, as detailed in the Appendix, relationships exist among the sub-block singular vectors and values, leading to the forms

$$\begin{aligned}
\mathbf{S}_{11} &= \mathbf{U}_{11}\boldsymbol{\Lambda}_{11}^{1/2}\mathbf{V}_{11}^H \\
\mathbf{S}_{12} &= -\mathbf{U}_{11}\boldsymbol{\Theta}^H\left(\mathbf{I} - \boldsymbol{\Lambda}_{11}\right)^{1/2}\mathbf{V}_{22}^H \\
\mathbf{S}_{21} &= \mathbf{U}_{22}\boldsymbol{\Theta}\left(\mathbf{I} - \boldsymbol{\Lambda}_{11}\right)^{1/2}\mathbf{V}_{11}^H \\
\mathbf{S}_{22} &= \mathbf{U}_{22}\boldsymbol{\Lambda}_{11}^{1/2}\mathbf{V}_{22}^H
\end{aligned} \quad (21)$$

where $\boldsymbol{\Theta}$ is a diagonal *phase shift* matrix with arbitrary complex elements of unit magnitude.

Given this framework, assume that a desired value of $\boldsymbol{\Gamma}_0$ has been provided. Using the form for $\boldsymbol{\Gamma}_0$ in (13) coupled with the expressions in (21) leads to

$$\begin{aligned}
\boldsymbol{\Gamma}_0 &= \mathbf{U}_0\boldsymbol{\Lambda}_0^{1/2}\mathbf{V}_0^H \\
&= \mathbf{U}_{22}\left[\boldsymbol{\Lambda}_{11}^{1/2} - \left(\mathbf{I} - \boldsymbol{\Lambda}_{11}\right)^{1/2}\mathbf{T}\left(\mathbf{I} - \boldsymbol{\Lambda}_{11}\right)^{1/2}\right]\mathbf{V}_{22}^H
\end{aligned} \quad (22)$$

$$\mathbf{T} = \boldsymbol{\Theta}\mathbf{V}_{11}^H\left(\mathbf{I} - \mathbf{S}_{RR}\mathbf{U}_{11}\boldsymbol{\Lambda}_{11}^{1/2}\mathbf{V}_{11}^H\right)^{-1}\mathbf{S}_{RR}\mathbf{U}_{11}\boldsymbol{\Theta}^H, \quad (23)$$

where the first equality is the SVD of $\boldsymbol{\Gamma}_0$. We have flexibility in choosing the singular vectors of $\mathbf{U}_{ii}$ and $\mathbf{V}_{ii}$, $i \in 1, 2$, and therefore will choose representations that lead to mathematical simplicity. First, we see that if $\mathbf{S}_{RR} = \mathbf{U}_{RR}\boldsymbol{\Lambda}_{RR}^{1/2}\mathbf{V}_{RR}^H$, then by choosing $\mathbf{U}_{11} = \mathbf{V}_{RR}$ and $\mathbf{V}_{11} = \mathbf{U}_{RR}$ we obtain

$$\mathbf{T} = \left(\mathbf{I} - \boldsymbol{\Lambda}_{RR}^{1/2}\boldsymbol{\Lambda}_{11}^{1/2}\right)^{-1}\boldsymbol{\Lambda}_{RR}^{1/2} \quad (24)$$

which is diagonal. If we further choose $\mathbf{U}_{22} = \mathbf{U}_0$ and $\mathbf{V}_{22} = \mathbf{V}_0$, we can solve (22) to obtain

$$\boldsymbol{\Lambda}_{11}^{1/2} = \left(\boldsymbol{\Lambda}_0^{1/2} + \boldsymbol{\Lambda}_{RR}^{1/2}\right)\left(\mathbf{I} + \boldsymbol{\Lambda}_0^{1/2}\boldsymbol{\Lambda}_{RR}^{1/2}\right)^{-1}. \quad (25)$$

The matrix $\boldsymbol{\Theta}$ is arbitrary for achieving the design goal provided it is diagonal with complex entries of unit magnitude, and we therefore use $\boldsymbol{\Theta} = j\mathbf{I}$.

We assume uncoupled amplifiers ($\mathbf{S}_{A,ij}$ and $\boldsymbol{\Gamma}_L$ are diagonal), so that typical design goals are achieved for diagonal $\boldsymbol{\Gamma}_0$. If $\Gamma_{\rm opt}$ and Γ_{MS} represent the (scalar) source reflection coefficient for achieving amplifier minimum noise figure and maximum power gain [17], respectively, then achieving these goals are accomplished by setting $\boldsymbol{\Gamma}_0 = \Gamma_{\rm opt}\mathbf{I}$ and $\boldsymbol{\Gamma}_0 = \Gamma_{MS}\mathbf{I}$. Since MIMO capacity depends on signal-to-noise ratio (SNR), we expect a design for minimum noise figure to outperform one for maximum power gain.

To achieve diagonal $\boldsymbol{\Gamma}_0$, the matching network must be coupled to "undo" the coupling created by the antenna, and it therefore acts as an *array combining network* as well as an impedance transforming network. To explore the implication of this observation, let $\mathbf{E}_R(\theta,\phi)$ represent the $2 \times N_R$ matrix with mth column $\mathbf{e}_{Rm}(\theta,\phi)$. Then, the matrix of effective radiation patterns observed at the matching network output ports can be constructed as

$$\mathbf{E}_2^T(\theta,\phi) = \frac{1}{2Z_0^{1/2}}\mathbf{G}(\mathbf{I}-\mathbf{S}_{RR})\mathbf{E}_R^T(\theta,\phi). \tag{26}$$

Then, following the development in Section II, we operate the array as a radiator with transmitted field $\mathbf{e}_R(\theta,\phi) = \mathbf{E}_R(\theta,\phi)\mathbf{i}_R$ and total transmitted power

$$P_R^{\rm inst} = \frac{1}{2\eta_0}\int \mathbf{e}_R^T(\theta,\phi)\mathbf{e}_R^*(\theta,\phi)d\Omega \tag{27}$$

where η_0 is the free-space impedance and Ω represents solid angle. Equating this expression to the radiated power computed using circuit theory (see (1)) yields

$$(\mathbf{I}-\mathbf{S}_{RR})\int \mathbf{E}_R^T(\theta,\phi)\mathbf{E}_R^*(\theta,\phi)d\Omega\,(\mathbf{I}-\mathbf{S}_{RR}^H) = 2\eta_0 Z_0\,(\mathbf{I}-\mathbf{S}_{RR}\mathbf{S}_{RR}^H) \tag{28}$$

where we have used that $\mathbf{i}_R = Z_0^{-1/2}(\mathbf{I}-\mathbf{S}_{RR})\mathbf{b}_1$ and $\mathbf{S}_{RR}^T = \mathbf{S}_{RR}$ by reciprocity.

Using these results with the matching network SVD relationships, it can be readily shown that the matrix

$$\mathbf{C} = \int \mathbf{E}_2^T(\theta,\phi)\mathbf{E}_2^*(\theta,\phi)d\Omega \tag{29}$$

is diagonal provided that $\boldsymbol{\Gamma}_0$ and therefore $\mathbf{U}_0$ are diagonal, which means that the effective radiation patterns seen at the matching network output are orthogonal. This result indicates that 1) the coupled antennas terminated with this matching network maintain unit radiation efficiency as demonstrated in [19], and 2) these virtual radiation patterns provide zero correlation in a propagation environment with full angle spread [4]. Because these patterns are formed by the coupling in the antennas and matching network before injection of the amplifier noise, the system can provide higher MIMO capacity than obtainable from uncoupled antennas without this network.

Finally, since designing coupled matching networks is highly complex, it is common to instead assume that the coupled antenna impedance can be adequately represented using only the diagonal elements of the full impedance matrix $\mathbf{Z}_{RR}$ to obtain $\overline{\mathbf{Z}}_{RR}$ and computing a diagonal $\overline{\mathbf{S}}_{RR}$ with elements $\overline{S}_{RR,ii} = (\overline{Z}_{RR,ii}-Z_0)/(\overline{Z}_{RR,ii}+Z_0)$. This value of $\overline{\mathbf{S}}_{RR}$ is then used in place of $\mathbf{S}_{RR}$ to specify an uncoupled matching network as outlined above. However, when analyzing the performance of such a match, the nondiagonal form of $\mathbf{S}_{RR}$ must be used in (20).

III. Coupled System Capacity

We will use capacity as a metric for comparing the performance of MIMO systems with different coupling levels and matching networks. This capacity is derived from the mutual information which, for the signal in (20) where both the transmit signal $\mathbf{a}_T$ and noise are drawn from zero-mean complex Gaussian distributions, assumes the form

$$I(\mathbf{v}_L,\mathbf{a}_T) = \log_2(\mathbf{R}_L) - \log_2(\mathbf{R}_N) \tag{30}$$

where $\mathbf{R}_L = E\{\mathbf{v}_L\mathbf{v}_L^H\}$ is the total voltage covariance and $\mathbf{R}_N$ is the noise covariance. We will construct each covariance matrix separately.

A. Noise Covariance

For the mth amplifier, the statistics of the noise waves $a_{\eta,m}$ and $b_{\eta,m}$ can be represented in terms of effective noise temperatures ($T_{\alpha,m}, T_{\beta,m}, T_{\Gamma,m} = T_{\gamma,m}e^{j\phi_{\gamma,m}}$) which are readily computed from other noise parameters [18]. If we assume identical amplifiers ($T_{\alpha,m} = T_\alpha$, etc.) and that the noise in each amplifier is statistically uncorrelated with that of all other amplifiers, then the noise satisfies

$$\begin{aligned} E\{\mathbf{a}_\eta\mathbf{a}_\eta^H\} &= k_B T_\alpha B\mathbf{I} \\ E\{\mathbf{b}_\eta\mathbf{b}_\eta^H\} &= k_B T_\beta B\mathbf{I} \\ E\{\mathbf{a}_\eta\mathbf{b}_\eta^H\} &= k_B T_\Gamma^* B\mathbf{I} \end{aligned} \tag{31}$$

where k_B is the Boltzmann constant and B is the system noise power bandwidth.

Using these results in conjunction with (20), the noise covariance can be expressed as

$$\mathbf{R}_N = \mathbf{Q}\mathbf{R}_\eta\mathbf{Q}^H \tag{32}$$

$$\begin{aligned} \mathbf{R}_\eta &= E\{(\boldsymbol{\Gamma}_0\mathbf{b}_\eta - \mathbf{a}_\eta)(\boldsymbol{\Gamma}_0\mathbf{b}_\eta - \mathbf{a}_\eta)^H\} \\ &= k_B B\underbrace{\left(T_\alpha\mathbf{I} + T_\beta\boldsymbol{\Gamma}_0\boldsymbol{\Gamma}_0^H - T_\Gamma\boldsymbol{\Gamma}_0 - T_\Gamma^*\boldsymbol{\Gamma}_0^H\right)}_{T_\alpha\mathbf{R}_{\eta o}} \end{aligned} \tag{33}$$

where we have factored out the constant T_α from $\mathbf{R}_{\eta o}$ so that the structure of $\mathbf{R}_{\eta o}$ is a function only of the relative values T_β/T_α and T_Γ/T_α. Using this representation, the absolute noise value controlled by $k_B B T_\alpha$ can be specified based on a desired SNR level.

B. Capacity

The matrix $\mathbf{R}_L$ represents the covariance of the received signal plus noise. Using the independence of the signal and noise waves, this matrix may be expressed as

$$\mathbf{R}_L = \mathbf{Q}\left[\mathbf{G}\mathbf{S}_{RT}\mathbf{R}_T\mathbf{S}_{RT}^H\mathbf{G}^H + \mathbf{R}_\eta\right]\mathbf{Q}^H \tag{34}$$

where $\mathbf{R}_T$ was introduced in (2). Using this result and (33), the mutual information in (30) becomes

$$I(\mathbf{v}_L, \mathbf{a}_T) = \log_2 \frac{|\mathbf{G}\mathbf{S}_{RT}\mathbf{R}_T\mathbf{S}_{RT}^H\mathbf{G}^H + \mathbf{R}_\eta|}{|\mathbf{R}_\eta|}. \tag{35}$$

Finally, if we compute the eigenvalue decomposition (EED) $\mathbf{R}_{\eta o} = \boldsymbol{\xi}_\eta \boldsymbol{\Lambda}_\eta \boldsymbol{\xi}_\eta^H$ where $\boldsymbol{\xi}_\eta$ is unitary, then the mutual information expression becomes

$$I(\mathbf{v}_L, \mathbf{a}_T) = \log_2 \left| \frac{\mathbf{Y}\mathbf{R}_T\mathbf{Y}^H}{k_B B T_\alpha} + \mathbf{I} \right| \tag{36}$$

where $\mathbf{Y} = \boldsymbol{\Lambda}_\eta^{-1/2}\boldsymbol{\xi}_\eta^H\mathbf{G}\mathbf{S}_{RT}$. The capacity results when the transmit covariance matrix $\mathbf{R}_T$ is specified according to the water-filling solution, with the total transmit power limited according to $\mathrm{Tr}(\mathbf{R}_T\mathbf{A}) \leq P_T$ as derived in (2). Because this power constraint is a departure from the typical constraint $\mathrm{Tr}(\mathbf{R}_T) \leq P_T$, the water-filling procedure must be modified, as detailed in [14], [20].

IV. Computational Examples

To demonstrate application of the analysis framework developed in this paper and to illustrate the impact of antenna coupling and amplifier matching on MIMO system capacity, we use a model problem consisting of two half-wave dipoles at transmit and receive. The simplicity of this problem allows us to accurately characterize the coupled antennas and draw basic conclusions concerning the system operation.

A. Antenna Electromagnetic Characterization

While closed-form expressions for coupled dipole impedance matrices exist (for reasonable antenna spacings), expressions for the patterns do not, motivating the use of full-wave electromagnetic solutions. Furthermore, simple thin-wire simulations assume that the current is independent of azimuthal angle around the wire, an assumption that is violated for very closely-spaced dipoles [21]–[23]. Since in this work it is desired to characterize the coupled antennas as the spacing is reduced to zero, we have chosen to use the finite-difference time-domain (FDTD) method [24], [25] to perform detailed simulations that return both S-parameter and radiation pattern descriptions for the dipole antennas. In this analysis, the z-oriented half-wave (total-length) dipoles with wire radius 0.01λ and separated by a distance d are located at the center of the computational domain. Because we are considering narrowband systems, single-frequency antenna excitation is used. The FDTD grid uses 80 cells per wavelength in the z direction and 200 cells per wavelength in the x and y directions. This finer resolution is required to adequately model the current variation as a function of azimuthal angle on the finite-radius wire for close antenna spacings. Because of the fine grid resolution, a relatively small buffer region of only a quarter wavelength (to minimize simulation memory) is placed between the antennas and the terminating 8-cell perfectly matched layer (PML) absorbing boundary condition (ABC). The impact of this small buffer region was investigated previously and shown to produce fractional errors below 10^{-4} relative to the results obtained for a half-wavelength thick buffer [14], [20].

B. Receive Amplifiers

The transistor used as the foundation for the amplifier in this work is a BJT taken from a Hewlett-Packard Application Note [26]. At a collector-emitter bias voltage of 10 V, collector current of 4 mA, frequency of 4 GHz, and reference impedance of $Z_0 = 50\,\Omega$, the S-parameters and noise parameters are given as

$$\begin{aligned} \mathbf{S}_{11} &= 0.552\angle 169^\circ & \mathbf{S}_{12} &= 0.049\angle 23^\circ \\ \mathbf{S}_{21} &= 1.681\angle 26^\circ & \mathbf{S}_{22} &= 0.839\angle -67^\circ \\ F_{\min} &= 2.5\ \mathrm{dB} & \Gamma_{\mathrm{opt}} &= 0.475\angle 166^\circ \\ R_n &= 3.5\,\Omega \end{aligned} \tag{37}$$

where $F_{\min}$, Γ_{opt}, and R_n represent the minimum noise figure, optimal source termination for noise figure, and effective noise resistance, respectively. These parameters are converted to the effective noise temperatures T_α, T_β, and T_Γ using standard techniques.

C. Capacity Results

We now explore the capacity of the model system under different matching goals. In these computations, 5,000 random realizations of a path-based, clustered channel model [27] are generated to create a set of transfer matrices $\mathbf{H}$ as in (5). Details on the implementation of this model, including the parameters used to model an indoor propagation environment, can be found in [28]. For each realization, we place single dipoles in the transmit and receive spaces and create a lossless receive matching network with $S_{11} = S_{RR}^*$ so that $\Gamma_0 = 0$ (all terms are scalars). We then can simplify the single-input single-output (SISO) SNR as

$$\mathrm{SNR}_S = \frac{|S_{RT}|^2}{1 - |S_{RR}|^2} \frac{P_T}{k_B B T_\alpha} \tag{38}$$

where P_T is the total transmit power. This SNR value is then averaged by moving each dipole in 0.1λ steps over a linear range of 1.5λ. For a given transmit power, the value of $k_B B T_\alpha$ can be computed to achieve an average SISO SNR (20 dB in this work) for the channel realization.

We next construct the matching network to achieve the specified design goal for each transmit/receive dipole spacing, as outlined in Section II-E. For each configuration, we compute the capacity averaged over the 5,000 channel matrices $\mathbf{H}$ with the corresponding noise power levels $k_B B T_\alpha$. The transmit array spacing is fixed at 0.5λ. In all plots, we use the abbreviations "NF" and "SI" to indicate matching for minimum noise figure or matching based on the self-impedance (diagonal $\overline{\mathbf{S}}_{RR}$), respectively. We also use "NC" to indicate that coupling is neglected at the receiver. For all cases, we use the same coupled transmit configuration to facilitate meaningful comparison of

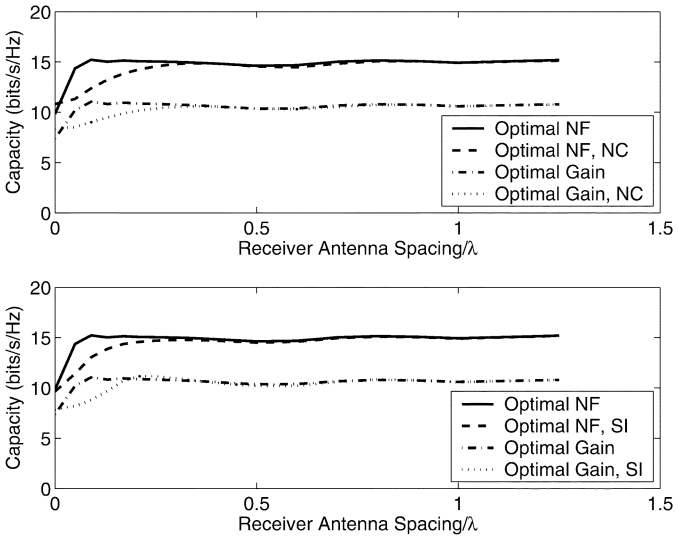

Fig. 3. Average capacity as a function of receive dipole separation with mutual coupling (optimal and self-impedance match) as well as without without mutual coupling. Matching for both minimum noise figure and maximum power gain are considered.

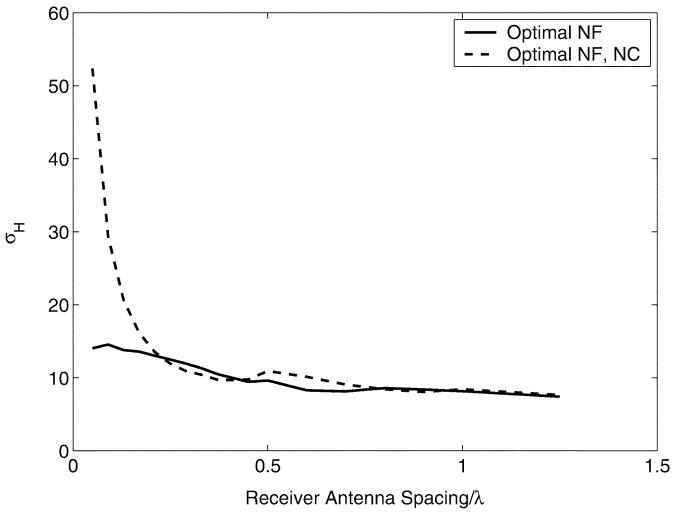

Fig. 4. Ratio of the largest to smallest singular values of the effective channel matrix as a function of receive dipole spacing for coupled and uncoupled receive antennas and an optimal noise figure match.

the results. Propagation is confined to the horizontal plane such that $\theta_{T\ell} = \theta_{R\ell} = \pi/2$. Since the dipoles and resulting currents are z-oriented, only the $\hat{\theta}$ polarization is required in the channel description in (5). For general antenna geometries that allow currents to flow in other directions, both polarizations should be included in the model.

Fig. 3 plots the capacity as a function of receive dipole spacing for matching networks that achieve minimum noise figure and maximum amplifier gain. Results for a coupled match and a simpler self-impedance match as well as for no receiver coupling are included. We first observe that the match achieving minimum amplifier noise figure (noise figure of $F = F_{\min} = 2.5$ dB) produces notably higher capacity than the match providing maximum power transfer which generates a much higher noise figure of $F = 7.2$ dB. This result is intuitive, since ultimately capacity depends on SNR as opposed to absolute signal strength. However, obtaining this result from simulation is enabled by the improved noise model implemented in this work. We also observe that for close antenna spacings with high coupling, the shortcomings of the self-impedance match are evident. However, once the spacing reaches approximately $d = \lambda/4$, this match provides near optimal performance.

We also observe from Fig. 3 that for small antenna spacings, coupled dipoles can have a higher capacity than uncoupled ones. This stems from the orthogonal radiation patterns observed at the matching network output as discussed in Section II-E. To explore this phenomenon further, we take the EED $\mathbf{A} = \boldsymbol{\xi}_A \boldsymbol{\Lambda}_A \boldsymbol{\xi}_A^H$ and, following the developments in [14], [20], construct the effective channel

$$\mathbf{H}_e = \boldsymbol{\Lambda}_\eta^{-1/2} \boldsymbol{\xi}_\eta^H \mathbf{G} \mathbf{S}_{RT} \boldsymbol{\xi}_A \boldsymbol{\Lambda}_A^{-1/2}. \tag{39}$$

Then, we define σ_H as the ratio of the largest to smallest singular values of $\mathbf{H}_e$, a metric that represents the relative quality of the two effective spatial channels. Fig. 4 plots this quantity averaged over the Monte Carlo channel realizations as a function of receive antenna spacing. As can be seen, the orthogonal radiation patterns of the *properly-terminated* coupled dipoles tend to more effectively equalize the quality of the two spatial channels (smaller σ_H), which increases MIMO capacity.

A variety of different conclusions concerning the relative performance of uncoupled and coupled antennas have appeared in recent literature. While many studies have demonstrated that coupling increases capacity [6]–[12], others have suggested that this is not the case [13]. First, we point out that none of these prior results have been generated using the model detail included here. Second, this performance enhancement requires an appropriate coupled matching network, which is impractical for most applications and therefore not considered in most prior studies. In fact, we have already observed that a more practical self-impedance match does not provide this benefit. Third, a notable recent study has demonstrated that packing an increasing number of dipoles into a linear array of a given aperture size leads to an increasing MIMO capacity unless coupling is included in the analysis [29]. This conclusion should not be viewed as inconsistent with the results included here, since in that case the number of dipoles is varied as the antenna aperture is fixed, while in this case the number of dipoles is fixed while the aperture is varied.

Because of the dependence of capacity on SNR, it is intriguing to consider the match achieving $\boldsymbol{\Gamma}_0 = \mathbf{0}$ which removes the noise term $\boldsymbol{\Gamma}_0 \mathbf{b}_\eta$ from (18) and for this device generates a noise figure of $F = 3$ dB (close to the minimum of $F_{\min} = 2.5$ dB). Fig. 5 compares the capacity of the system using this matching network with that obtained using the other matching criteria. As expected, for this device the performance for $\boldsymbol{\Gamma}_0 = \mathbf{0}$ is very close to that obtained for a match achieving minimal noise figure.

V. Conclusion

This paper has outlined a procedure for analyzing capacity performance of MIMO systems with mutually-coupled antenna arrays. The formulation includes a realistic noise model for the

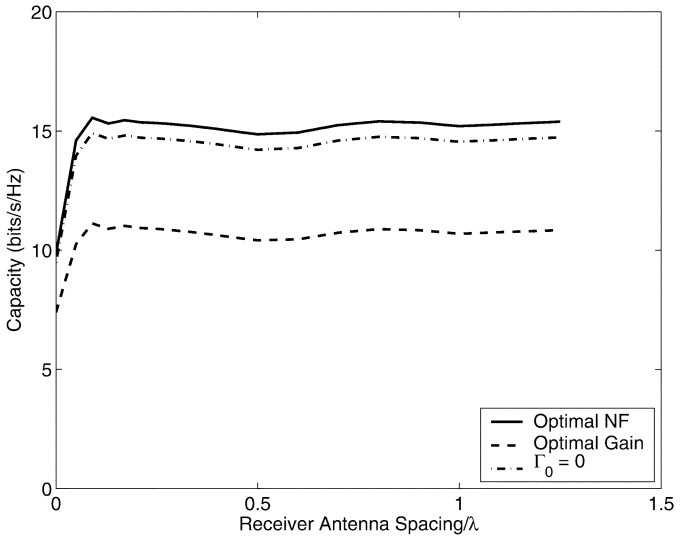

Fig. 5. Average capacity as a function of receive dipole separation for coupled antennas with matching networks that achieve minimum noise figure, maximum power gain, and zero output reflection.

receiving amplifiers and facilitates a careful examination of the system end-to-end performance. The framework also allows specification of the matching network transfer properties to achieve different design goals and includes a radiated power constraint based on the coupled transmit array characteristics. Representative computations for a 2×2 MIMO system employing coupled dipole antennas and a realistic front-end amplifier transistor illustrate the performance differences associated with different matching network goals as well as different coupling assumptions. The key conclusion drawn from these results is that matching for minimum noise figure is superior to matching for maximum power transfer.

APPENDIX

Lossless matching networks are characterized by unitary S-matrices such that $\mathbf{S}_M^H \mathbf{S}_M = \mathbf{I}$. Using the representation in (11) and substituting the SVD of the sub-blocks $\mathbf{S}_{ij} = \mathbf{U}_{ij} \mathbf{\Lambda}_{ij}^{1/2} \mathbf{V}_{ij}^H$ into the lossless constraint yields the relations

$$\mathbf{V}_{ij} \mathbf{\Theta}_{ij} = \mathbf{V}_{jj} \quad \mathbf{\Lambda}_{ij} = \mathbf{I} - \mathbf{\Lambda}_{jj} \quad i \neq j \tag{40}$$

where $\mathbf{\Theta}_{ij}$ is a diagonal matrix with unit-magnitude entries. This operation also produces the condition

$$\mathbf{\Lambda}_{11}^{1/2} \mathbf{U}_{11}^H \mathbf{U}_{12} (\mathbf{I} - \mathbf{\Lambda}_{22})^{1/2} \mathbf{\Theta}_{12} = -\mathbf{\Theta}_{21}^H (\mathbf{I} - \mathbf{\Lambda}_{11})^{1/2} \mathbf{U}_{21}^H \mathbf{U}_{22} \mathbf{\Lambda}_{22}^{1/2}. \tag{41}$$

There is an entire family of matching networks that satisfy these conditions. Since we are only interested in finding one lossless matching network that achieves specified design goals, we can further specify the singular vectors/values. In this spirit, we choose $\mathbf{U}_{12} = \mathbf{U}_{11}$ and $\mathbf{U}_{21} = \mathbf{U}_{22}$. Then, according to (41) we obtain $\mathbf{\Theta}_{21} = -\mathbf{\Theta}_{12}^H = \mathbf{\Theta}$ and $\mathbf{\Lambda}_{22} = \mathbf{\Lambda}_{11}$. The sub-blocks of $\mathbf{S}_M$ can then be expressed as in (21).

REFERENCES

[1] G. J. Foschini and M. J. Gans, "On limits of wireless communications in a fading environment when using multiple antennas," *Wireless Personal Commun.*, vol. 6, pp. 311–335, Mar. 1998.
[2] G. G. Raleigh and J. M. Cioffi, "Spatio-temporal coding for wireless communication," *IEEE Trans. Commun.*, vol. 46, pp. 357–366, Mar. 1998.
[3] C. A. Balanis, *Antenna Theory: Analysis and Design*. New York: Wiley, 1997.
[4] R. G. Vaughan and J. B. Andersen, "Antenna diversity in mobile communications," *IEEE Trans. Veh. Technol.*, vol. VT-36, pp. 147–172, Nov. 1987.
[5] R. R. Ramirez and F. De Flaviis, "A mutual coupling study of linear polarized microstrip antennas for use in BLAST wireless communications architecture," in *Proc. IEEE Antennas and Propag. Society Int. Symp.*, vol. 2, Salt Lake City, UT, Jul. 16–21, 2000, pp. 490–493.
[6] J. Luo, J. R. Zeidler, and S. McLaughlin, "Performance analysis of compact antenna arrays with MRC in correlated Nakagami fading channels," *IEEE Trans. Veh. Technol.*, vol. 50, pp. 267–277, Jan. 2001.
[7] T. Svantesson and A. Ranheim, "Mutual coupling effects on the capacity of multielement antenna systems," in *Proc. IEEE Int. Conf. Acoustics, Speech, and Signal Processing*, vol. 4, Salt Lake City, UT, May 7–11, 2001, pp. 2485–2488.
[8] M. Stoytchev, H. Safar, A. L. Moustakas, and S. Simon, "Compact antenna arrays for MIMO applications," in *Proc.IEEE Antennas and Propag. Society Int. Symp.*, vol. 3, Boston, MA, Jul. 8–13, 2001, pp. 708–711.
[9] C. Waldschmidt, J. v. Hagen, and W. Wiesbeck, "Influence and modeling of mutual coupling in MIMO and diversity systems," in *Proc. IEEE Antennas and Propag. Society Int. Symp.*, vol. 3, San Antonio, TX, Jun. 16–21, 2002, pp. 190–193.
[10] M. C. Leifer, "Signal correlations in coupled cell and MIMO antennas," in *Proc. IEEE Antennas and Propag. Society Int. Symp.*, vol. 3, San Antonio, TX, June 16–21, 2002, pp. 194–197.
[11] B. Clerckx, D. Vanhoenacker-Janvier, C. Oestges, and L. Vandendorpe, "Mutual coupling effects on the channel capacity and the space-time processing of MIMO communication systems," in *Proc. IEEE Int. Conf. Commun.*, vol. 4, Anchorage, AK, May 11–15, 2003, pp. 2638–2642.
[12] V. Jungnickel, V. Pohl, and C. von Helmolt, "Capacity of MIMO systems with closely spaced antennas," *IEEE Commun. Lett.*, vol. 7, pp. 361–363, Aug. 2003.
[13] P. N. Fletcher, M. Dean, and A. R. Nix, "Mutual coupling in multi-element array antennas and its influence on MIMO channel capacity," *Electron. Lett.*, vol. 39, pp. 342–344, Feb. 2003.
[14] J. W. Wallace and M. A. Jensen, "The capacity of MIMO wireless systems with mutual coupling," in *Proc. IEEE 56th Veh. Technol. Conf.*, vol. 2, Vancouver, British Columbia, Canada, Sep. 24–28, 2002, pp. 696–700.
[15] C. Waldschmidt, C. Kuhnert, S. Schulteis, and W. Wiesbeck, "Analysis of compact arrays for MIMO based on a complete RF system model," in *Proc. IEEE Topical Conf. Wireless Commun. Tech.*, Honolulu, HI, Oct. 15–17, 2003.
[16] D. M. Pozar, *Microwave Engineering*. New York: Wiley, 1998.
[17] G. Gonzalez, *Microwave Transistor Amplifiers*. Englewood Cliffs, NJ: Prentice-Hall, 1997.
[18] J. Engberg and T. Larsen, *Noise Theory of Linear and Nonlinear Circuits*. New York: Wiley, 1995.
[19] S. Stein, "On cross coupling in multiple-beam antennas," *IRE Trans. Antennas Propag.*, vol. 10, pp. 548–557, Sep. 1962.
[20] J. W. Wallace and M. A. Jensen, "Mutual coupling in MIMO wireless systems: A rigorous network theory analysis ," *IEEE Trans. Wireless Commun.*, vol. 3, pp. 1317–1325, Jul. 2004.
[21] A. C. Ludwig, "Wire-grid modeling of surfaces," *IEEE Trans. Antennas Propagat.*, vol. AP-35, pp. 1045–1048, Sep. 1987.
[22] C. W. Trueman and S. J. Kubina, "Verifying wire-grid model integrity with program 'CHECK'," *Appl. Comput. Electromagn. Soc. J.*, vol. 5, no. 2, pp. 17–17, Winter 1990.
[23] J. W. Rockway, J. C. Logan, D. W. S. Tam, and S. T. Li, *The MININEC System: Microcomputer Analysis of Wire Antennas*. Norwood, MA: Artech House, 1988.
[24] M. A. Jensen and Y. Rahmat-Samii, "Performance analysis of antennas for hand-held transceivers using FDTD," *IEEE Trans. Antennas Propagat.*, vol. 42, pp. 1106–1113, Aug. 1994.
[25] A. Taflove and S. C. Hagness, *Computational Electrodynamics: The Finite-Difference Time-Domain Method*, Second ed. Boston: Artech House, 2000.

[26] "A Low Noise 4 GHz Transistor Amplifier Using the HXTR-6101 Silicon Bipolar Transistor," Hewlett-Packard, Hewlett-Packard Application Note 967, 1975.
[27] Q. H. Spencer, B. D. Jeffs, M. A. Jensen, and A. L. Swindlehurst, "Modeling the statistical time and angle of arrival characteristics of an indoor multipath channel," *IEEE J. Sel. Areas Commun.*, vol. 18, pp. 347–360, Mar. 2000.
[28] J. W. Wallace and M. A. Jensen, "Modeling the indoor MIMO wireless channel," *IEEE Trans. Antennas Propag.*, vol. 50, pp. 591–599, May 2002.
[29] R. Janaswamy, "Effect of element mutual coupling on the capacity of fixed length linear arrays," *IEEE Antennas Wireless Propag. Lett.*, vol. 1, no. 1, pp. 157–160, 2002.

Matthew L. Morris received the B.S. degree in physics from Brigham Young University, Provo, UT, in 2000 and is currently working toward the Ph.D. degree in electrical engineering at the same university.

His research interests include MIMO communication with an emphasis on channel capacity.

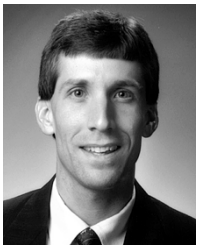

Michael A. Jensen (S'93–M'95–SM'01) received the B.S. (*summa cum laude*) and M.S. degrees in electrical engineering from Brigham Young University (BYU), Provo, UT, in 1990 and 1991, respectively, and the Ph.D. in electrical engineering from the University of California, Los Angeles (UCLA), in 1994.

From 1989 to 1991, he was a Graduate Research Assistant in the Lasers and Optics Laboratory, BYU. From 1991 to 1994, he was a Graduate Student Researcher in the Antenna Laboratory, UCLA. Since 1994, he has been at the Electrical and Computer Engineering Department, BYU, where he is currently an Associate Professor. His main research interests include antennas and propagation for personal communications, microwave circuit design, radar remote sensing, numerical electromagnetics, and optical fiber communications.

Dr. Jensen is a Member of Eta Kappa Nu and Tau Beta Pi. In 1990, he received a National Science Foundation Graduate Fellowship. He was awarded the best student paper award at the 1994 IEEE International Symposium on Antennas and Propagation, and received the Harold A. Wheeler Applications Prize Paper Award in the IEEE TRANSACTIONS ON ANTENNAS AND PROPAGATION in 2002. He currently serves on the Joint Meetings Committee for the IEEE Antennas and Propagation Society and as an Associate Editor for the IEEE TRANSACTIONS ON ANTENNAS AND PROPAGATION. He was the Technical Program Chair for the 2000 IEEE International Symposium on Antennas and Propagation and the General Co-Chair for the IEEE Topical Conference on Wireless Communications in 2003.